


## ORIGINAL ARTICLE

# Association Between Earliest Amyloid Uptake and Functional Connectivity in Cognitively Unimpaired Elderly

Andreas Hahn<sup>1</sup>, Tor O. Strandberg<sup>2</sup>, Erik Stomrud<sup>2</sup>, Markus Nilsson<sup>3</sup>, Danielle van Westen<sup>4,5</sup>, Sebastian Palmqvist<sup>2,6</sup>, Rik Ossenkoppele <sup>2,7</sup> and Oskar Hansson<sup>2</sup>

<sup>1</sup>Department of Psychiatry and Psychotherapy, Medical University of Vienna, AT-1090, Austria, <sup>2</sup>Clinical Memory Research Unit, Department of Clinical Sciences, Malmö, Lund University, SE-22100, Sweden, <sup>3</sup>Lund University Bioimaging Center, Lund University, Lund, SE-22100, Sweden, <sup>4</sup>Department of Clinical Sciences Lund, Diagnostic Radiology, Lund University, SE-22100, Sweden, <sup>5</sup>Imaging and Function, Skåne University Health Care, Lund, SE-20502, Sweden, <sup>6</sup>Department of Neurology, Skåne University Hospital, SE-20502, Sweden and <sup>7</sup>Department of Neurology and Alzheimer Center, Neuroscience Campus Amsterdam, VU University Medical Center, Amsterdam, NL-1081 HV, The Netherlands

Address correspondence to Oskar Hansson, Memory Clinic, Skåne University Hospital, SE-20502 Malmö, Sweden. E-mail: oskar.hansson@med.lu.se

## Abstract

Alterations in cognitive performance have been noted in nondemented subjects with elevated accumulation of amyloid- $\beta$  (A $\beta$ ) fibrils. However, it is not yet understood whether brain function is already influenced by A $\beta$  deposition during the very earliest stages of the disease. We therefore investigated associations between [<sup>18</sup>F]Flutemetamol PET, resting-state functional connectivity, gray and white matter structure and cognitive performance in 133 cognitively normal elderly that exhibited normal global A $\beta$  PET levels. [<sup>18</sup>F]Flutemetamol uptake in regions known to accumulate A $\beta$  fibrils early in preclinical AD (i.e., mainly certain parts of the default-mode network) was positively associated with dynamic but not static functional connectivity ( $r = 0.77$ ). Dynamic functional connectivity was further related to better cognitive performance ( $r = 0.21$ – $0.72$ ). No significant associations were found for A $\beta$  uptake with gray matter volume or white matter diffusivity. The findings demonstrate that the earliest accumulation of A $\beta$  fibrils is associated with increased functional connectivity, which occurs before any structural alterations. The enhanced functional connectivity may reflect a compensatory mechanism to maintain high cognitive performance in the presence of increasing amyloid accumulation during the earliest phases of AD.

**Key words:** [<sup>18</sup>F]flutemetamol, Alzheimer's disease, dynamic connectivity, resting-state fMRI

As one of the main causes of dementia, Alzheimer's disease (AD) is characterized by the accumulation of amyloid  $\beta$  (A $\beta$ ) and

hyperphosphorylated tau in the brain as major neuropathological hallmarks (Spelting et al. 2011). This leads to neuronal

dysfunction and ultimately cell death, which is clinically accompanied by progressive cognitive decline such as memory impairment and executive dysfunction (Buckner 2004; Braskie and Thompson 2013).

Since the neuropathological changes occur many decades before the manifestation of clinical symptoms (Sperling et al. 2014), early detection may offer an essential aspect in disease prevention. Biomarkers obtained from cerebrospinal fluid (CSF) and positron emission tomography (PET) imaging are often routinely used when classifying subjects as amyloid positive or negative (Blennow et al. 2015; Palmqvist et al. 2015). Although CSF markers detect amyloid abnormalities slightly earlier than PET (Palmqvist et al. 2016a), CSF A $\beta$  seems to plateau earlier during the nondementia stage of AD where PET amyloid accumulation still increases (Villemagne et al. 2013; Palmqvist et al. 2016b), possibly because they represent different aspects of the pathology (Mattsson et al. 2015; Palmqvist et al. 2016a). Furthermore, whole brain imaging has the advantage of regional specificity, enabling PET imaging to grade the amount of amyloid burden at a more detailed level than global CSF markers (Palmqvist et al. 2014).

In addition to A $\beta$  PET, also other imaging modalities have provided great insight into the disease progress of AD. Previous work focusing on AD patients has shown that brain metabolism (Ossenkoppele et al. 2012), neuronal activation (Golby et al. 2005), resting-state functional connectivity (Nuttall et al. 2016), and brain structure (Jin et al. 2017) deteriorate across the AD spectrum. To further investigate brain alterations in prodromal stages of AD, various studies have been carried out in mild cognitive impairment and healthy elderly subjects with mixed results. Interestingly, several studies examining nondemented populations have observed associations of A $\beta$  accumulation with increases in brain function and connectivity (Sperling et al. 2003; Mormino et al. 2011; Lim et al. 2014), which is often interpreted as a potential compensatory mechanism. It is important to note that the vast majority of these studies included subjects already exhibiting increased and widespread neocortical A $\beta$  pathology. Given that deposition of A $\beta$  fibrils is considered to represent one of the earliest changes in AD (Sperling et al. 2011), which is believed to begin at least 1–2 decades before dementia onset (Bateman et al. 2012; Buchhave et al. 2012;

Jansen et al. 2015), it is crucial to consider amyloid status when targeting the early onset stage. Recent investigations of nondemented individuals have identified the brain regions that are most prone to exhibit increased A $\beta$  accumulation in the earliest stages of AD, and these regions mainly include certain parts of the default mode (DM) network (Villeneuve et al. 2015; Gonneaud et al. 2017; Palmqvist et al. 2017). However, further studies are needed to determine whether this very early accumulation of A $\beta$  fibrils affects brain connectivity, structure and function.

To this end, we evaluated the associations of amyloid ([ $^{18}$ F] Flutemetamol) PET uptake in the brain regions with earliest A $\beta$  deposition with functional connectivity, gray matter volume, white matter diffusivity and cognitive performance in nondemented individuals with an overall negative amyloid PET scan (i.e., they exhibited both a normal neocortical composite SUVR and normal visual read). Considering that functional connectivity exhibits nonstationary characteristics over time (Hutchison et al. 2013; Calhoun et al. 2014), this was further split into different dynamic states. Dynamic functional connectivity has been demonstrated to represent behaviorally relevant information (Jia et al. 2014) and to differ between various mental disorders (Li et al. 2014; Yu et al. 2015), but its relation to amyloid pathology has not yet been assessed.

## Methods

### Subjects

In the present study we included 133 nondemented elderly subjects, consisting of 85 healthy subjects and 48 with subjective cognitive decline (SCD) from the Swedish BioFINDER study (<http://biofinder.se>). All cases were without clinically relevant amyloid deposition (i.e., all were PET negative subjects, see definition below). See Table 1 for demographic details. Details about study design, methods, and specific inclusion/exclusion criteria of the BioFINDER study have previously been described (Janelidze et al. 2016, 2017; Palmqvist et al. 2017). In the present study the following cognitive tests were included: Mini Mental State Examination (MMSE) as a measure of global cognition, the 10-word delayed recall part of the Alzheimer's Disease Assessment Scale, cognitive subscale (ADAS-cog) as a measure of memory performance, and A Quick Test of cognitive speed (AQT), color-form version as a measure of cognitive speed and attention. All participants provided written informed consent after detailed explanation of the study protocol. The study was approved by the Ethical Review Board of Lund University and all procedures were performed according to the Declaration of Helsinki.

### Positron Emission Tomography

To assess A $\beta$  accumulation in the brain, PET imaging was carried out as described previously (Palmqvist et al. 2014, 2017). Briefly, all subjects underwent a PET examination with [ $^{18}$ F] Flutemetamol on a Philips Gemini TF 16 scanner (Philips Healthcare). The radioligand represents an  $^{18}$ F-labeled analog to [ $^{11}$ C]PiB, where both bind specifically to A $\beta$  (Vandenberghe et al. 2010; Heurling et al. 2015). The mean injected dose was 185 MBq and PET images were acquired 90–110 min postinjection (5 min per frame), followed by a CT scan for attenuation correction. Image processing included movement correction, averaging across time and spatial normalization to MNI-space (Palmqvist et al. 2017). Standard uptake value ratio (SUVR) images were computed using a combined reference region (whole cerebellum, pons/brainstem, eroded subcortical white matter) (Landau et al. 2015). Correction for partial volume

**Table 1** Demographic details (mean  $\pm$  sd). The sample comprised healthy controls (HC) and those with subjective cognitive decline (SCD). All participants had an MMSE score  $\geq$  25 and did not exhibit clinically relevant amyloid deposition (i.e., PET negative). [ $^{18}$ F] Flutemetamol SUVR, standard uptake value ratios of brain regions prone to early amyloid uptake (Fig. 1); MMSE, mini mental state examination score. Delayed recall, 10-word delayed recall part of the Alzheimer's disease assessment scale (number of errors out of 10); AQT, a quick test of cognitive speed color-form version (reaction time in seconds); APOE  $\epsilon$ 4, carriers of 1 or 2 alleles; History, family history of dementia in first degree relatives

	HC	SCD	All
n	85	48	133
Sex (m/f)	32/53	20/28	52/81
Age (years)	73.7 $\pm$ 4.2	68.9 $\pm$ 5.5	72.0 $\pm$ 5.2
[ $^{18}$ F] Flutemetamol SUVR	0.58 $\pm$ 0.06	0.61 $\pm$ 0.06	0.59 $\pm$ 0.06
MMSE	29.0 $\pm$ 1.0	28.9 $\pm$ 1.4	29.0 $\pm$ 1.2
Delayed recall (errors)	1.8 $\pm$ 1.9	2.7 $\pm$ 2.0	2.1 $\pm$ 2.0
AQT (s)	66.5 $\pm$ 12.6	72.3 $\pm$ 24.9	68.6 $\pm$ 18.1
Education (years)	11.8 $\pm$ 3.1	13.8 $\pm$ 3.1	12.5 $\pm$ 3.2
APOE $\epsilon$ 4 (%)	20.0	29.2	23.3
History (%)	30.6	47.9	36.8

effects was carried out with the geometric transfer matrix method (Rousset et al. 1998) by calculating and inverting the transfer matrix between tissue regions extracted from FreeSurfer segmentation. This correction step ensures that our results are not driven by potential differences in gray matter volume. All subjects showed normal A $\beta$  accumulation, that is, they were PET negative (PET $-$ ) according to a recently described classification (Palmqvist et al. 2017). In short, SUVR values of a neocortical composite region (frontal, lateral parietal, lateral temporal, anterior cingulate, posterior cingulate, precuneus) (Mormino et al. 2009) were required to be  $<0.759$  as defined with a mixture modeling analysis in a larger sample of the BioFINDER study ( $n = 406$ ). SUVR images were then masked by a conservative gray matter template (Yeo et al. 2011). Furthermore, all PET images were visually inspected by 3 experienced external physicians (at MNI, New Haven, USA), who independently classified all PET images as positive or negative. The physicians were blind to clinical data and the scans rated here were part of a larger data collection which included many positive cases as well. The final classification was obtained by majority rule, where at least 2 of the 3 physicians rated a subject as negative.

To evaluate associations between A $\beta$  accumulation and MR imaging parameters, we extracted the average [ $^{18}$ F]Flutemetamol SUVR from brain regions that are most prone to the earliest accumulation of A $\beta$  (Fig. 1a in Palmqvist et al. 2017). The regions comprised the posterior cingulate cortex and precuneus, the subgenual part of the anterior cingulate cortex and to a lesser extent bilaterally the angular gyrus, posterior middle temporal gyrus and middle frontal gyrus (Fig. 1,  $P < 0.05$  FWE-corrected voxel level, which is more stringent than previously published (Palmqvist et al. 2017) to focus on regions with strongest changes). The regions are similar to those observed as the most affected early A $\beta$ -positive regions in autosomal dominant AD (Tang et al. 2016). Furthermore, the regions correspond to those classified as early (stage 2) A $\beta$  progression (Grothe et al. 2017) and show substantial overlap with another study assessing early stages of A $\beta$  deposition (Villeneuve et al. 2015). Since these brain regions largely comprise the DM network we also extracted SUVR values explicitly from the DM as defined in a low (7 networks) and high resolution (17 networks) parcellation of the brain (Yeo et al. 2011).

### Magnetic Resonance Imaging

Magnetic resonance imaging (MRI) was carried out with a 3 T Siemens Tim Trio scanner (Siemens Medical Solutions,

Erlangen, Germany). This included acquisition of a T1-weighted structural MRI (magnetization prepared rapid gradient echo sequence, TE/TR = 3.37/1950 ms,  $1 \times 1 \times 1.2$  mm $^3$ ), diffusion weighted images (single-shot echo planar imaging sequence, TE/TR = 86/8200 ms, 64 diffusion encoding directions at  $b = 1000$  s/mm $^2$  and one image at  $b = 0$  s/mm $^2$ ,  $2 \times 2 \times 2$  mm $^3$ ) as well as 6 min functional MRI at resting-state with eyes closed (gradient-recalled echo planar imaging, TE/TR = 30/2000 ms,  $3 \times 3 \times 3$  mm $^3$ ).

### Voxel-Based Morphometry

T1-weighted images were segmented and spatially normalized to MNI-space with the CAT12 toolbox (<http://www.neuro.uni-jena.de/cat/>) for SPM12 (<http://www.fil.ion.ucl.ac.uk/spm/>) using default parameters. Gray matter segments were converted to gray matter volume by multiplication with the Jacobian determinants to adjust for effects of nonlinear deformations. The final images were smoothed with an 8 mm Gaussian kernel.

### Diffusion Tensor Imaging

Diffusion weighted images were processed with FSL (<https://fsl.fmrib.ox.ac.uk/fsl/fslwiki/>), which included correction for eddy currents and movement, brain extraction and estimation of the tensor. This resulted in images representing mean diffusivity and fractional anisotropy (FA). Spatial normalization was carried out using tract based spatial statistics (TBSS) (Smith et al. 2006) with default parameters. Here, the individual FA images were nonlinearly registered to MNI-space and a white matter skeleton was created where FA images were mapped to. Images of mean diffusivity were normalized with the transformations obtained from the FA processing step.

### Static Functional Connectivity

fMRI data processing was carried out as described recently (Palmqvist et al. 2017) and included processing with FSL, AFNI (<https://afni.nimh.nih.gov/>), ANTS (<https://sourceforge.net/projects/advants/>), and Matlab (The Mathworks, Natick, MA). Functional images were corrected for slice timing differences and head motion. Confounding signals were removed by linear regression against signals from CSF and white matter, 6 components of physiological noise (Behzadi et al. 2007) and 24 motion parameters (Friston et al. 1996). Finally, a band-pass filter was applied ( $0.01 < f < 0.1$  Hz). Processed images were then transformed to MNI-space. Since subject motion is an essential issue

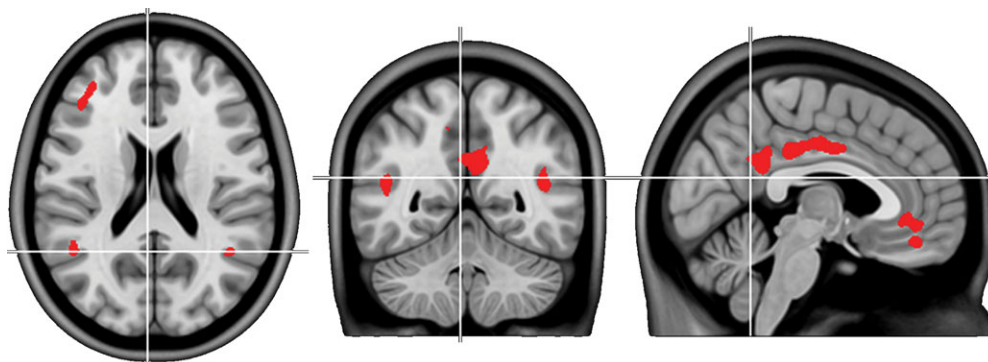


**Figure 1.** Brain regions which are most prone to earliest amyloid accumulation as identified in a recent analysis of the ADNI cohort ( $P < 0.05$  FWE-corrected voxel level) (Palmqvist et al. 2017). The average [ $^{18}$ F]Flutemetamol SUVR across these regions was extracted for each subject and used for further analysis.

in resting-state fMRI analyses, all subjects exceeding a frame-wise displacement of 0.6 mm on average and 3 mm at maximum were removed (Power et al. 2012). Another precaution was included in this elderly population by summing up the voxel-to-voxel BOLD signal correlations across the entire brain. Outliers in this metric most likely reflect motion-related global signal confounds and were thus removed (He and Liu 2012). The 133 subjects stated above already represent the final sample after applying these exclusion criteria. Finally, fMRI frames were censored if they constituted outliers in the total signal frame-to-frame variation (75% plus 1.5 times interquartile range).

Static functional connectivity matrices were computed by cross-correlation of the entire BOLD signal time courses between each region of interest pair. Brain regions were defined using a publicly available atlas of 840 regions based on resting-state fMRI data (Craddock et al. 2012). This represents a detailed parcellation of the human brain close to a voxel-wise analysis but with the advantage of processing a computationally feasible amount of data. The resulting correlation values were then z-transformed with Fisher's *r*-to-*z* transformation.

### Dynamic Functional Connectivity

Data processing was identical as for the static analysis until the calculation of connectivity matrices. Dynamic functional connectivity was computed for the symmetric matrix defined by the  $840 \times 840$  region pairs using an exponentially tapered sliding window approach (Zalesky et al. 2014). The weighting step assigns highest weights to the most recent events and the exponential smoothing avoids sudden changes in functional connectivity, making it less susceptible to outlier values. The time window for each dynamic connectivity matrix was  $N = 60$  s (Zalesky et al. 2014) and the weight vector was defined as an exponential function (Pozzi et al. 2012):

$$w_t = w_0 * e^{(t-N)/\theta}$$

with  $t = 1 \dots N$  and  $w_0$  being

$$w_0 = (1 - e^{-1/\theta}) / (1 - e^{-N/\theta})$$

where the exponent  $\theta$  was set to 1/3 of the window length (Zalesky et al. 2014). Weighted Pearson's correlation coefficients were then computed from weighted means, standard deviation, and covariances, followed by z-transformation. Dynamic functional connectivity matrices across time were computed by consecutively shifting the time window by 1 TR. The values for the exponent (Pozzi et al. 2012) and window length (Hutchison et al. 2013; Allen et al. 2014) were based on previous reports (Zalesky et al. 2014) as it was demonstrated that these represent reasonable choices.

### Identification of Dynamic Connectivity States

Dynamic functional connectivity is characterized by repeatedly occurring states (Zalesky et al. 2014). To identify these different connectivity states, *k*-means clustering was carried out with Matlab using dynamic functional connectivity matrices of all subjects as features and 1-correlation as similarity metric (Hutchison et al. 2013; Allen et al. 2014). For the clustering, connectivity matrices were thresholded at a network density of 20% (i.e., only keeping the strongest 20% of connections) to avoid influence of spurious correlations (Zalesky et al. 2014). Clustering

was repeated for a variable number of clusters ( $k = 2-10$  and  $10-20$  with steps = 1 and 2, respectively). The optimal solution across all clustering results was determined by the elbow criterion (Allen et al. 2014), where the within sum of squares did not show a marked improvement anymore for a higher number of clusters. For each subject multiple occurrences of a certain state were averaged for further statistical evaluation.

Due to previous concerns of clustering sliding window correlations (Keogh and Lin 2005), the cluster centroids obtained from dynamic functional connectivity were compared with centroids of random connectivity matrices. For computational reasons this procedure was carried out with a randomly selected subset of the total sample ( $n = 43$ ), for  $k = 6$  clusters and 3 repeats with random initial centroids. Since the similarity metric was 1-correlation, we also used the correlation to compute the within- and between-cluster distance.

Furthermore, sliding window correlations were also computed with a window of  $N = 46$  s as this represents the middle of previously proposed window lengths of 30–60 s (Shirer et al. 2012; Hutchison et al. 2013). The resulting states were then compared with those obtained with the  $N = 60$  s window.

### Statistical Analysis

Associations between [ $^{18}$ F]Flutemetamol SUVR, MR imaging parameters, cognitive test scores (MMSE, AQT, ADAS-cog), years of education, and first degree family history of dementia were calculated with linear regression analysis. For whole-brain static and dynamic functional connectivity the Network Based Statistics (NBS) toolbox (Zalesky et al. 2010) was used. To control for false positives within whole-brain connectivity matrices of 840 regions, the initial connection threshold was set to  $P < 0.0001$  uncorrected, followed by a network threshold of  $P < 0.05$  FWE corrected. Hence, all *P*-values provided in the results are FWE corrected. Statistical testing was done with 5000 random permutations and intensity weighting (i.e., weighting by connection strength). In other words, the total intensity (i.e., the sum of *t*-values of suprathreshold links) of an observed network component was compared with a permutation generated null distribution of component intensities, thereby assigning an FWE-corrected *P*-value to the observed network component. To calculate *r*-values for significant associations, the functional connections of the significant network components were weighted by *t*-values, averaged for each subject and correlated with the variable of interest. The extracted network components which showed a significant association with [ $^{18}$ F]Flutemetamol SUVR, where also correlated with cognitive test scores. SPM12 and FSL were used to compute whole-brain regressions with gray matter volume ( $P < 0.05$  FWE-corrected voxel level, cluster extent  $>10$  voxels) and white matter diffusion parameters (500 random permutations,  $P < 0.05$  FWE-corrected with threshold free cluster enhancement), respectively. In order to obtain more generalizable results of an elderly population independent of potential confounders and risk factors, all statistical analyses were corrected for sex, age, clinical diagnosis (healthy, SCD), and APOE  $\epsilon 4$  status (noncarriers vs. carriers of 1 or 2 alleles). Visualization of connectograms and brain networks was carried out with Circos (Krzywinski et al. 2009) and BrainNet Viewer (Xia et al. 2013), respectively. For the connectograms each element of a  $840 \times 840$  connectivity matrix was allocated to 1 of 7 cortical resting-state networks (DA, dorsal attention; DM, default mode; FP, frontoparietal; FT, frontotemporal; SM, somatomotor; VA, ventral attention; VI, visual) (Yeo et al.

2011), the basal ganglia (BG), the amygdala/hippocampus (HI), or the cerebellum (CER) from the Harvard–Oxford atlas as included in FSL.

## Results

We have recently identified the cortical regions most prone to accumulate A $\beta$  fibrils during the earliest stages of AD (Palmqvist et al. 2017) (Fig. 1). In the current study the average [ $^{18}$ F]Flutemetamol SUVR was extracted from these regions in 133 nondemented and A $\beta$  PET negative cases from the BioFINDER cohort.

### Static Functional Connectivity

The [ $^{18}$ F]Flutemetamol uptake in the early A $\beta$  regions did not show an association with static functional connectivity. This was also not the case when extracting [ $^{18}$ F]Flutemetamol SUVR from the high or low resolution DM defined by Yeo et al. (2011) or when using SUVRs from the neocortical composite score (Mormino et al. 2011).

### Dynamic Functional Connectivity

K-means clustering identified 6 dynamic connectivity states as best solution, which is similar to previous studies (Allen et al. 2014; Yu et al. 2015). All states exhibited a common backbone of links (calculated as the average across all subjects and states), which was characterized by strong within network connections as well as default mode, dorsal attention, ventral attention, and somatomotor connections with other networks (Fig. 2). The common backbone almost perfectly reflected the average static functional connectivity pattern with  $r = 0.97$  between the  $840 \times 840$  matrices (both thresholded at a network density of 20%, Fig. 2). Furthermore, each of the 6 states exhibited connections, which were specific to itself (i.e.,  $>2$  SD stronger than average). State 1 showed additional links of the default mode, visual and cerebellar networks. State 2 exhibited frontoparietal connections and default mode links with other networks. In state 3, connections of the ventral attention network were dominant. State 4 showed strong somatomotor links. States 5 and 6 were mostly characterized by default mode connections.

Detailed evaluation of sliding window correlations showed good similarity of cluster centroids within functional connectivity data ( $r = 0.82 \pm 0.05$ ), which was markedly different to random matrices ( $r = 0.002 \pm 0.0004$ ). This indicates that clustering obtained from sliding window correlations of dynamic functional connectivity data is clearly different to that of random data (Keogh and Lin 2005). Changing the sliding window to  $N = 45$  s also showed high reproducibility of the functional connectivity states ( $r = 0.97 \pm 0.02$ ).

Of the 6 dynamic states, only functional connectivity of state 1 was positively associated with [ $^{18}$ F]Flutemetamol SUVR in the early A $\beta$  region ( $r = 0.77$ , Fig. 3). The correlation featured strong default mode connections with the ventral attention and somatomotor networks as well as between the ventral attention and visual networks and comprised 122 regions (out of 840) and 145 edges. Additionally correcting for individual gray matter volume of the early A $\beta$  region ( $r = 0.77$ ), global white matter hyperintensity volume ( $r = 0.77$ ), Fazekas score ( $r = 0.76$ ) or Wahlund score ( $r = 0.76$ ) did not affect this relationship. The connections, which were associated with SUVR, were also related to a better MMSE score ( $r = 0.21$ , Fig. 3). Extracting

SUVR from the DM (Yeo et al. 2011) showed a significant association with functional connectivity of state 1 for the low ( $r = 0.70$ , 75 regions, 87 edges) and high resolution parcellations ( $r = 0.71$ , 71 regions, 82 edges). No significant correlation was observed for SUVRs from the neocortical composite score. Further exploratory whole-brain correlations with cognitive test scores were found for state 3 ( $r = 0.51$ , VI–SM connections) and 6 with higher MMSE scores ( $r = 0.50$ , CER–VA, and CER–SM connections) and for state 3 with ADAS error rate ( $r = -0.72$ , FT–VA, and FT–SM connections).

### Structural MRI

No significant associations were found between [ $^{18}$ F]Flutemetamol uptake in the early A $\beta$  region and any regional gray matter volumes or any of the regional white matter diffusion parameters (mean diffusivity, FA).

## Discussion

Proceeding from brain regions previously identified as the most susceptible to the earliest amyloid deposition (Palmqvist et al. 2017), we here demonstrated robust positive associations of [ $^{18}$ F]Flutemetamol amyloid uptake in these regions with resting-state fMRI functional connectivity in a large sample of nondemented elderly subjects of the BioFINDER study. Importantly, the sample comprised only PET negative subjects, that is, those without clinically relevant global amyloid deposition and a negative visual read, and the observed associations were independent of confounding factors such as age, sex, APOE  $\epsilon 4$  status, presence of SCD, and structural alterations. These findings suggest that the very earliest accumulation of A $\beta$  fibrils are biologically relevant and indeed affect brain function.

Interestingly, only dynamic but not static functional connectivity was associated with A $\beta$  uptake. This indicates that static functional connectivity analysis exhibits decreased sensitivity when capturing the association in the earliest stages of A $\beta$  accumulation. Hence, separating the different dynamic functional states may offer increased ability to detect alterations in brain connectivity as compared with the commonly used approach of temporally static connectivity, since the latter may simply represent an average of the different dynamic states (Jin et al. 2017). This is confirmed by the remarkable match between static functional connectivity and average dynamic connectivity observed here ( $r = 0.97$ ). Accordingly, dynamic functional connectivity has been shown to outperform static one with respect to patient classification in post-traumatic stress disorder (Jin et al. 2017).

Most studies of functional connectivity in AD focused on the DM, due to the large overlap with A $\beta$  accumulation (Buckner et al. 2009). A recent study identified the posterior DM as initially failing region and its connectivity with other hubs being associated with A $\beta$  accumulation (Jones et al. 2016). However, the earliest deposition of A $\beta$  also comprises other networks such as the frontoparietal, dorsal and ventral attention. (Palmqvist et al. 2017). In line with this, the neocortical composite score did not yield significant correlations and extraction of [ $^{18}$ F]Flutemetamol SUVR from the entire DM resulted in a substantially smaller network, which emphasizes the relevance of regional specificity (Palmqvist et al. 2016b). The overlap of early A $\beta$  deposition and the DM is characterized in further detail by the current work. We indeed confirm that mainly DM connections are involved, but it seems that links to other

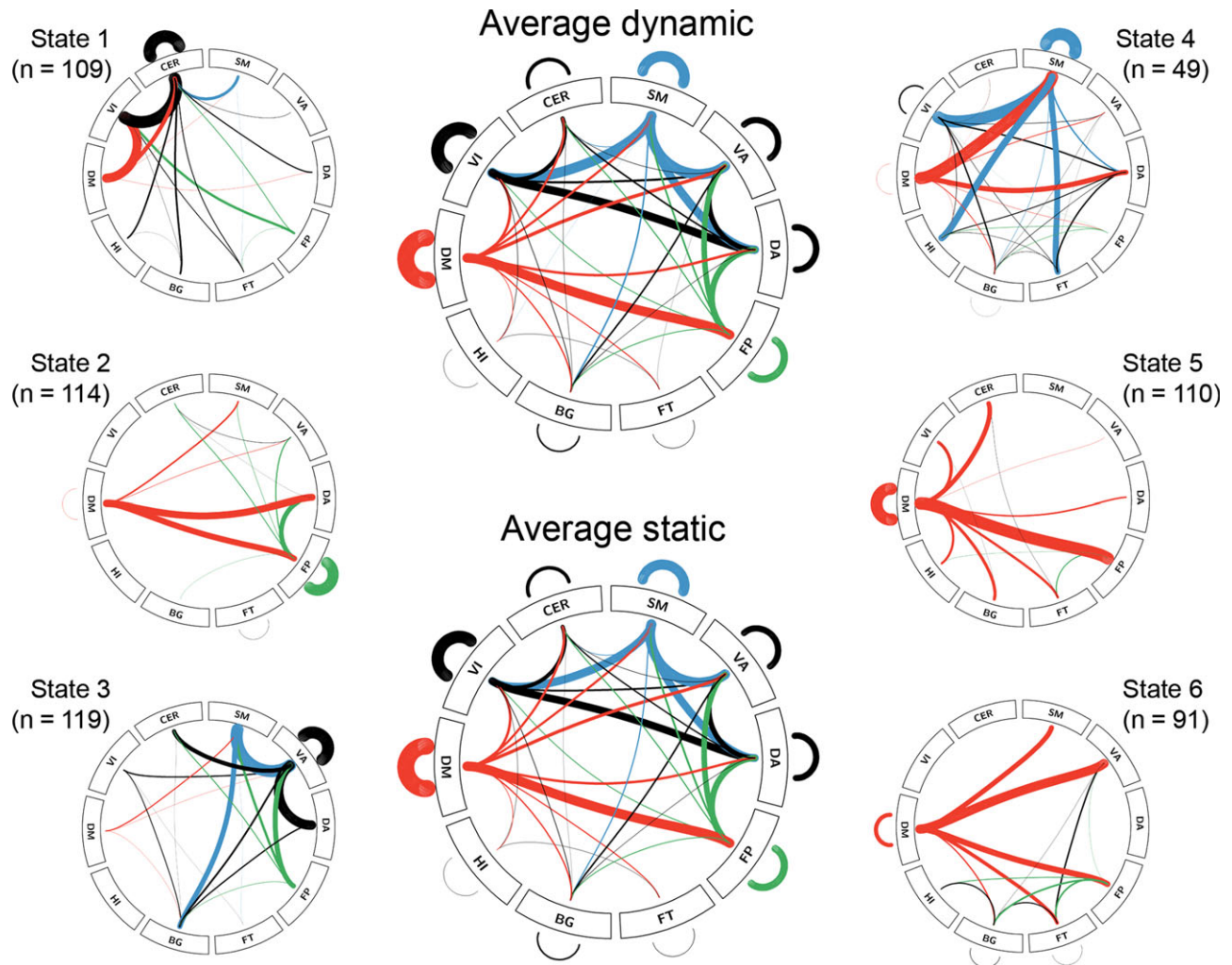


**Figure 2.** Dynamic functional connectivity states and number of subjects exhibiting each state (total sample  $n = 133$ ). Average static (and dynamic) connections across all subjects (and states) showed strong overlap ( $r = 0.97$ ). For each of the 6 states only those connections are shown, which are stronger than the common ones (i.e.,  $>2$  standard deviations stronger than the average). Line thickness is proportional to connectivity strength (z-score). Line thickness of average connections is down-scaled by 200 for visualization and only the strongest 20% of connections are shown. See Figure 3 for abbreviations and color code.

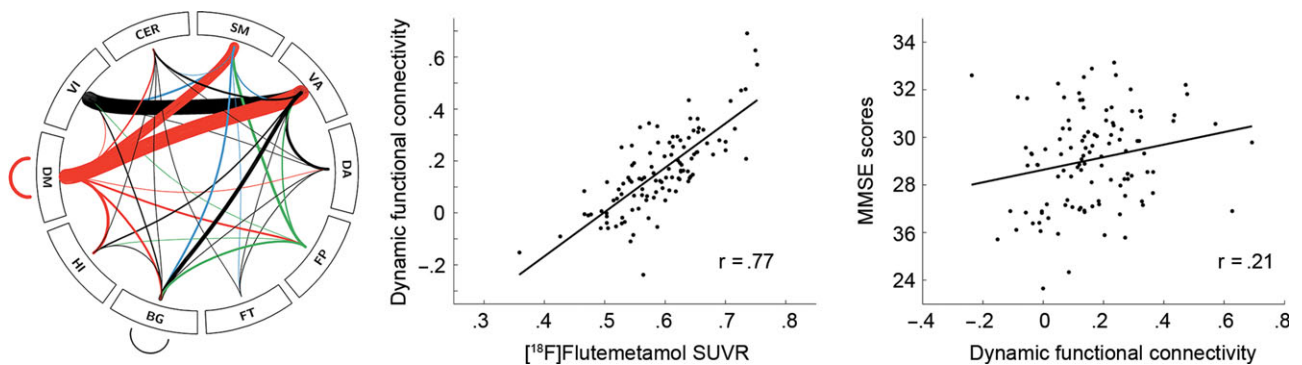


**Figure 3.** Associations between  $[^{18}\text{F}]$ Flutemetamol SUVR extracted from regions shown in Fig. 1 and dynamic resting-state functional connectivity, adjusted for the covariates sex, age, APOE  $\epsilon 4$  status and presence of SCD ( $P < 0.05$  FWE corrected). Functional connectivity further showed a positive correlation with MMSE scores. Line thickness in connectogram is proportional to association strength (t-values). The  $r$ -values denote Pearson correlation coefficients after correction for covariates using regression. After correction the original mean values were added to the residuals to approximate the raw values, thus calculated values are relative and may exceed the maximum of the MMSE. BG, basal ganglia; CER, cerebellum; DA, dorsal attention; DM, default mode (red); FP, frontoparietal (green); FT, frontotemporal; HI, amygdala-hippocampus; SM: somatomotor (blue); VA, ventral attention; VI, visual.

networks rather than within-network connections are predominantly affected by the earliest A $\beta$  fibril burden (Brier et al. 2012; Elman et al. 2016). This indicates that global network coordination appears to be more important than local circuit functioning in the pathophysiology of AD.

Similar to the topology of earliest A $\beta$  deposition (Palmqvist et al. 2017), the positively associated functional connections were also characterized by links of the DM with the ventral attention network. These findings are in line with previously reported increases of neuronal activation (Elman et al. 2014) and functional connectivity (Mormino et al. 2011; Elman et al. 2016) in healthy elderly subjects with increased amyloid binding. More importantly, the regions and networks involved in the earliest stages also match those that are affected as the disease progresses eventually into Alzheimer's dementia (Brier et al. 2014; Elman et al. 2016), despite the fact that all subjects studied here were nondemented and yet without clinically relevant A $\beta$  uptake. Furthermore, the increases in functional connectivity were independent of any structural alterations since no comparable relationships were observed for A $\beta$  uptake with any regional gray or white matter changes. It therefore seems that changes in functional connectivity occur before structural deteriorations in the early stages of pathology of AD.

Increased functional connectivity is usually related to better cognitive performance (Hampson et al. 2006; Zhang et al. 2014). Accordingly, the higher dynamic functional connectivity, which were correlated with early A $\beta$  accumulation, were also associated with better global cognitive function (i.e., higher MMSE scores). The trimodal relationships between amyloid uptake (in the early A $\beta$  region), functional connectivity and cognitive performance could reflect a potential compensatory mechanism, a commonly observed manifestation of cognitive reserve in early stages of dementia (Buckner 2004; Stern 2012; Amieva et al. 2014; Ossenkoppele et al. 2014), where enhanced brain function compensates for amyloid-induced neuronal damage and structural deterioration later in the disease. The phenomenon has been observed across a wide range of imaging modalities, including neuronal activation (Sole-Padulles et al. 2009; Elman et al. 2014), functional (Palmqvist et al. 2017; Serra et al. 2017), and metabolic connectivity (Perani et al. 2017) and even for gray matter volume (van Loenhoud et al. 2017). Hence, there is great amount of work suggesting that subjects with better cognitive performance also exhibit an increased ability to recruit neuronal networks in order to counterbalance the increased amyloid burden. In line with this, our data might indicate that the increased functional connectivity is more common in individuals with a greater cognitive reserve. As the main novel finding, we demonstrate that these mechanisms are already at play when global A $\beta$  uptake is still within the normal range, thereby possibly capturing the earliest manifestations of cognitive reserve as a response to emerging pathological processes. The importance to assess early A $\beta$  accumulation has also recently been confirmed, as this can be detected in cognitively normal subjects (Gonneaud et al. 2017; Grothe et al. 2017; Hanseeuw et al. 2018), it is associated with increased tau deposition (Leal et al. 2018) and with subsequent memory decline (Farrell et al. 2018; Landau et al. 2018).

On the other hand, the recruitment of additional networks could also imply that these subjects are more affected by AD pathology. The increased connectivity would then allow subjects in the early disease stages to tolerate a higher amount of amyloid deposition while maintaining high cognitive function (Stern 2012) as it was also shown with the current findings. These compensatory mechanisms may however fail with

further disease progression and when pathology overwhelms function. The view of initially high cognitive performance but rapid decrease afterwards is supported by several studies, particularly with respect to functional connectivity, suggesting an inverted U-shape of cognitive function. That is, functional connectivity of different brain networks has been shown to first increase with increasing yet normal brain amyloid accumulation while maintaining high cognitive function, but then again decreases as amyloid reaches abnormal levels (Damoiseaux et al. 2012; Brier et al. 2014; Palmqvist et al. 2017; Schultz et al. 2017). Hence, a key aspect of future research will be to identify the individual time point of this deterioration and to establish potentially preventive interventions.

Finally, we would like to add an alternative explanation, as increased connectivity may also reflect hyperintense synchronous activity, which in turn regulates A $\beta$  accumulation (Bero et al. 2011; Ovsepian and O'Leary 2016). Longitudinal studies are however required to clarify the exact underlying causes of the observed alterations.

The strength of the present study is the collection of a wide variety of imaging and cognitive measures in a large sample of A $\beta$ -negative nondemented individuals. A limitation is that 6 min of resting state fMRI is on the lower boundary to assess dynamic functional connectivity (but similar (Jin et al. 2017) or even shorter durations have been used previously (Allen et al. 2014; Braun et al. 2015; Yu et al. 2015)). Hence, it is possible that the scan time was simply too short since not all subjects experienced every state. However, there was no difference for subjects who did or did not exhibit state 1 regarding amyloid SUVR or cognitive test scores. Furthermore, it has been shown that 60 s windows (Hutchison et al. 2013) (or even 30 s (Braun et al. 2015)) are sufficiently long to evaluate dynamic connectivity, which yields up to 150 states per subject and on average 25 occurrences of each state.

Although the MMSE is not a particularly sensitive test in normal subjects, it is highly reliable and represents a standard assessment to test cognitive function. As such it is also part of a test battery that is widely used in preclinical AD including clinically normal elderly individuals (Donohue et al. 2014).

## Conclusion

We demonstrate that amyloid-related effects on dynamic functional connectivity already occur at the earliest stage of the disease, namely, in nondemented elderly subjects without clinically relevant global amyloid deposition and these effects are independent of structural alterations in gray and white matter. The enhanced functional connectivity may represent a compensatory mechanism to maintain cognitive function despite increasing amyloid pathology. Future research is needed to examine whether changes in functional connectivity may be clinically relevant to predict individual decline in cognitive function and disease progression.

## Funding

Work at the authors' research centers was supported by the European Research Council, the Swedish Research Council, the Strategic Research Area MultiPark (Multidisciplinary Research in Parkinson's disease) at Lund University, the Swedish Brain Foundation, the Swedish Alzheimer Association, the Knut and Alice Wallenberg Foundation, the Marianne and Marcus Wallenberg Foundation, Kockska Stiftelsen, the Skåne University Hospital Foundation, and the Swedish federal government

under the ALF agreement. [<sup>18</sup>F]Flutemetamol was provided by GE Healthcare. The visual reads of all PET images were funded by Roche.

## Conflict of interest

A.H., O.T.S., E.S., M.S., D.v.W., S.P., and R.O. have no conflicts of interest. O.H. has acquired research support (for the institution) from Roche, GE Healthcare, Biogen, AVID Radiopharmaceuticals, Fujirebio, and Euroimmun. In the past 2 years, he has received consultancy/speaker fees (paid to the institution) from Lilly, Roche, and Fujirebio.

## Notes

We thank G.M. James for data analysis support. *Conflict of Interest*: None declared.

## References

- Allen EA, Damaraju E, Plis SM, Erhardt EB, Eichele T, Calhoun VD. 2014. Tracking whole-brain connectivity dynamics in the resting state. *Cereb Cortex*. 24:663–676.
- Amieva H, Mokri H, Le Goff M, Meillon C, Jacqmin-Gadda H, Foubert-Samier A, Orgogozo JM, Stern Y, Dartigues JF. 2014. Compensatory mechanisms in higher-educated subjects with Alzheimer's disease: a study of 20 years of cognitive decline. *Brain*. 137:1167–1175.
- Bateman RJ, Xiong C, Benzinger TL, Fagan AM, Goate A, Fox NC, Marcus DS, Cairns NJ, Xie X, Blazey TM, et al. 2012. Clinical and biomarker changes in dominantly inherited Alzheimer's disease. *N Engl J Med*. 367:795–804.
- Behzadi Y, Restom K, Liu J, Liu TT. 2007. A component based noise correction method (CompCor) for BOLD and perfusion based fMRI. *Neuroimage*. 37:90–101.
- Bero AW, Yan P, Roh JH, Cirrito JR, Stewart FR, Raichle ME, Lee JM, Holtzman DM. 2011. Neuronal activity regulates the regional vulnerability to amyloid-beta deposition. *Nat Neurosci*. 14:750–756.
- Blennow K, Mattsson N, Scholl M, Hansson O, Zetterberg H. 2015. Amyloid biomarkers in Alzheimer's disease. *Trends Pharmacol Sci*. 36:297–309.
- Braskie MN, Thompson PM. 2013. Understanding cognitive deficits in Alzheimer's disease based on neuroimaging findings. *Trends Cogn Sci*. 17:510–516.
- Braun U, Schafer A, Walter H, Erk S, Romanczuk-Seiferth N, Haddad L, Schweiger JI, Grimm O, Heinz A, Tost H, et al. 2015. Dynamic reconfiguration of frontal brain networks during executive cognition in humans. *Proc Natl Acad Sci USA*. 112:11678–11683.
- Brier MR, Thomas JB, Ances BM. 2014. Network dysfunction in Alzheimer's disease: refining the disconnection hypothesis. *Brain Connect*. 4:299–311.
- Brier MR, Thomas JB, Snyder AZ, Benzinger TL, Zhang D, Raichle ME, Holtzman DM, Morris JC, Ances BM. 2012. Loss of intranetwork and internetwork resting state functional connections with Alzheimer's disease progression. *J Neurosci*. 32:8890–8899.
- Buchhave P, Minthon L, Zetterberg H, Wallin AK, Blennow K, Hansson O. 2012. Cerebrospinal fluid levels of beta-amyloid 1–42, but not of tau, are fully changed already 5 to 10 years before the onset of Alzheimer dementia. *Arch Gen Psychiatry*. 69:98–106.
- Buckner RL. 2004. Memory and executive function in aging and AD: multiple factors that cause decline and reserve factors that compensate. *Neuron*. 44:195–208.
- Buckner RL, Sepulcre J, Talukdar T, Krienen FM, Liu H, Hedden T, Andrews-Hanna JR, Sperling RA, Johnson KA. 2009. Cortical hubs revealed by intrinsic functional connectivity: mapping, assessment of stability, and relation to Alzheimer's disease. *J Neurosci*. 29:1860–1873.
- Calhoun VD, Miller R, Pearlson G, Adali T. 2014. The chronnectome: time-varying connectivity networks as the next frontier in fMRI data discovery. *Neuron*. 84:262–274.
- Craddock RC, James GA, Holtzheimer PE 3rd, Hu XP, Mayberg HS. 2012. A whole brain fMRI atlas generated via spatially constrained spectral clustering. *Hum Brain Mapp*. 33:1914–1928.
- Damoiseaux JS, Prater KE, Miller BL, Greicius MD. 2012. Functional connectivity tracks clinical deterioration in Alzheimer's disease. *Neurobiol Aging*. 33(828):e819–e830.
- Donohue MC, Sperling RA, Salmon DP, Rentz DM, Raman R, Thomas RG, Weiner M, Aisen PS. 2014. The preclinical Alzheimer cognitive composite: measuring amyloid-related decline. *JAMA Neurol*. 71:961–970.
- Elman JA, Madison CM, Baker SL, Vogel JW, Marks SM, Crowley S, O'Neil JP, Jagust WJ. 2016. Effects of beta-amyloid on resting state functional connectivity within and between networks reflect known patterns of regional vulnerability. *Cereb Cortex*. 26:695–707.
- Elman JA, Oh H, Madison CM, Baker SL, Vogel JW, Marks SM, Crowley S, O'Neil JP, Jagust WJ. 2014. Neural compensation in older people with brain amyloid-beta deposition. *Nat Neurosci*. 17:1316–1318.
- Farrell ME, Chen X, Rundle MM, Chan MY, Wig GS, Park DC. 2018. Regional amyloid accumulation and cognitive decline in initially amyloid-negative adults. *Neurology*. 91:e1809–e1821.
- Friston KJ, Williams S, Howard R, Frackowiak RS, Turner R. 1996. Movement-related effects in fMRI time-series. *Magn Reson Med*. 35:346–355.
- Golby A, Silverberg G, Race E, Gabrieli S, O'Shea J, Knierim K, Stebbins G, Gabrieli J. 2005. Memory encoding in Alzheimer's disease: an fMRI study of explicit and implicit memory. *Brain*. 128:773–787.
- Gonneaud J, Arenaza-Urquijo EM, Mezenge F, Landeau B, Gaubert M, Bejanin A, de Flores R, Wirth M, Tomadesso C, Poinsin G, et al. 2017. Increased florbetapir binding in the temporal neocortex from age 20 to 60 years. *Neurology*. 89:2438–2446.
- Grothe MJ, Barthel H, Sepulcre J, Dyrba M, Sabri O, Teipel SJ, Alzheimer's Disease Neuroimaging I. 2017. In vivo staging of regional amyloid deposition. *Neurology*. 89:2031–2038.
- Hampson M, Driesen NR, Skudlarski P, Gore JC, Constable RT. 2006. Brain connectivity related to working memory performance. *J Neurosci*. 26:13338–13343.
- Hanseeuw BJ, Betensky RA, Mormino EC, Schultz AP, Sepulcre J, Becker JA, Jacobs HIL, Buckley RF, LaPoint MR, Vannini P, et al. 2018. PET staging of amyloidosis using striatum. *Alzheimers Dement*. 14:1281–1292.
- He H, Liu TT. 2012. A geometric view of global signal confounds in resting-state functional MRI. *Neuroimage*. 59:2339–2348.
- Heurling K, Buckley C, Van Laere K, Vandenberghe R, Lubberink M. 2015. Parametric imaging and quantitative analysis of the PET amyloid ligand [(18)F]flutemetamol. *Neuroimage*. 121:184–192.
- Hutchison RM, Womelsdorf T, Allen EA, Bandettini PA, Calhoun VD, Corbetta M, Della Penna S, Duyn JH, Glover GH,



- Gonzalez-Castillo J, et al. 2013. Dynamic functional connectivity: promise, issues, and interpretations. *Neuroimage*. 80: 360–378.
- Janelidze S, Hertze J, Nagga K, Nilsson K, Nilsson C, Wennstrom M, van Westen D, Blennow K, Zetterberg H, Hansson O. 2017. Increased blood-brain barrier permeability is associated with dementia and diabetes but not amyloid pathology or APOE genotype. *Neurobiol Aging*. 51:104–112.
- Janelidze S, Zetterberg H, Mattsson N, Palmqvist S, Vanderstichele H, Lindberg O, van Westen D, Stomrud E, Minthon L, Blennow K, et al. 2016. CSF Abeta42/Abeta40 and Abeta42/Abeta38 ratios: better diagnostic markers of Alzheimer disease. *Ann Clin Transl Neurol*. 3:154–165.
- Jansen WJ, Ossenkoppele R, Knol DL, Tijms BM, Scheltens P, Verhey FR, Visser PJ, Aalten P, Aarsland D, Alcolea D, et al. 2015. Prevalence of cerebral amyloid pathology in persons without dementia: a meta-analysis. *J Am Med Assoc*. 313: 1924–1938.
- Jia H, Hu X, Deshpande G. 2014. Behavioral relevance of the dynamics of the functional brain connectome. *Brain Connect*. 4:741–759.
- Jin Y, Huang C, Daianu M, Zhan L, Dennis EL, Reid RI, Jack CR Jr., Zhu H, Thompson PM. 2017a. 3D tract-specific local and global analysis of white matter integrity in Alzheimer's disease. *Hum Brain Mapp*. 38:1191–1207.
- Jin C, Jia H, Lanka P, Rangaprakash D, Li L, Liu T, Hu X, Deshpande G. 2017b. Dynamic brain connectivity is a better predictor of PTSD than static connectivity. *Hum Brain Mapp*. 38:4479–4496.
- Jones DT, Knopman DS, Gunter JL, Graff-Radford J, Vemuri P, Boeve BF, Petersen RC, Weiner MW, Jack CR Jr., Alzheimer's Disease Neuroimaging I. 2016. Cascading network failure across the Alzheimer's disease spectrum. *Brain*. 139:547–562.
- Keogh E, Lin J. 2005. Clustering of time-series subsequences is meaningless: implications for previous and future research. *Knowl Inf Syst*. 8:154–177.
- Krzywinski M, Schein J, Biroi I, Connors J, Gascoyne R, Horsman D, Jones SJ, Marra MA. 2009. Circos: an information aesthetic for comparative genomics. *Genome Res*. 19:1639–1645.
- Landau SM, Fero A, Baker SL, Koeppe R, Mintun M, Chen K, Reiman EM, Jagust WJ. 2015. Measurement of longitudinal beta-amyloid change with 18F-florbetapir PET and standardized uptake value ratios. *J Nucl Med*. 56:567–574.
- Landau SM, Horng A, Jagust WJ, Alzheimer's Disease Neuroimaging I. 2018. Memory decline accompanies sub-threshold amyloid accumulation. *Neurology*. 90:e1452–e1460.
- Leal SL, Lockhart SN, Maass A, Bell RK, Jagust WJ. 2018. Subthreshold amyloid predicts tau deposition in aging. *J Neurosci*. 38:4482–4489.
- Li X, Zhu D, Jiang X, Jin C, Zhang X, Guo L, Zhang J, Hu X, Li L, Liu T. 2014. Dynamic functional connectomics signatures for characterization and differentiation of PTSD patients. *Hum Brain Mapp*. 35:1761–1778.
- Lim HK, Nebes R, Snitz B, Cohen A, Mathis C, Price J, Weissfeld L, Klunk W, Aizenstein HJ. 2014. Regional amyloid burden and intrinsic connectivity networks in cognitively normal elderly subjects. *Brain*. 137:3327–3338.
- Mattsson N, Insel PS, Donohue M, Landau S, Jagust WJ, Shaw LM, Trojanowski JQ, Zetterberg H, Blennow K, Weiner MW. 2015. Independent information from cerebrospinal fluid amyloid-beta and florbetapir imaging in Alzheimer's disease. *Brain*. 138:772–783.
- Mormino EC, Kluth JT, Madison CM, Rabinovici GD, Baker SL, Miller BL, Koeppe RA, Mathis CA, Weiner MW, Jagust WJ. 2009. Episodic memory loss is related to hippocampal-mediated beta-amyloid deposition in elderly subjects. *Brain*. 132:1310–1323.
- Mormino EC, Smiljic A, Hayenga AO, Onami SH, Greicius MD, Rabinovici GD, Janabi M, Baker SL, Yen IV, Madison CM, et al. 2011. Relationships between beta-amyloid and functional connectivity in different components of the default mode network in aging. *Cereb Cortex*. 21:2399–2407.
- Nuttall R, Pasquini L, Scherr M, Sorg C. 2016. Degradation in intrinsic connectivity networks across the Alzheimer's disease spectrum. *Alzheimers Dement (Amst)*. 5:35–42.
- Ossenkoppele R, Madison C, Oh H, Wirth M, van Berckel BN, Jagust WJ. 2014. Is verbal episodic memory in elderly with amyloid deposits preserved through altered neuronal function? *Cereb Cortex*. 24:2210–2218.
- Ossenkoppele R, Tolboom N, Foster-Dingley JC, Adriaanse SF, Boellaard R, Yaqub M, Windhorst AD, Barkhof F, Lammertsma AA, Scheltens P, et al. 2012. Longitudinal imaging of Alzheimer pathology using [11C]PIB, [18F]FDDNP and [18F]FDG PET. *Eur J Nucl Med Mol Imaging*. 39:990–1000.
- Ovsepian SV, O'Leary VB. 2016. Neuronal activity and amyloid plaque pathology: an update. *J Alzheimers Dis*. 49:13–19.
- Palmqvist S, Mattsson N, Hansson O. 2016a. Cerebrospinal fluid analysis detects cerebral amyloid-beta accumulation earlier than positron emission tomography. *Brain*. 139:1226–1236.
- Palmqvist S, Mattsson N, Hansson O. 2016b. Reply: Do we still need positron emission tomography for early Alzheimer's disease diagnosis? *Brain*. 139:e61.
- Palmqvist S, Schöll M, Strandberg O, Mattsson N, Stomrud E, Zetterberg H, Blennow K, Landau S, Jagust W, Hansson O. 2017. Earliest accumulation of  $\beta$ -amyloid occurs within the default-mode network and concurrently affects brain connectivity. *Nat Commun*. 8:1214.
- Palmqvist S, Zetterberg H, Blennow K, Vestberg S, Andreasson U, Brooks DJ, Owenius R, Hagerstrom D, Wollmer P, Minthon L, et al. 2014. Accuracy of brain amyloid detection in clinical practice using cerebrospinal fluid beta-amyloid 42: a cross-validation study against amyloid positron emission tomography. *JAMA Neurol*. 71:1282–1289.
- Palmqvist S, Zetterberg H, Mattsson N, Johansson P, Minthon L, Blennow K, Olsson M, Hansson O. 2015. Detailed comparison of amyloid PET and CSF biomarkers for identifying early Alzheimer disease. *Neurology*. 85:1240–1249.
- Perani D, Farsad M, Ballarini T, Lubian F, Malpetti M, Fracchetti A, Magnani G, March A, Abutaleb J. 2017. The impact of bilingualism on brain reserve and metabolic connectivity in Alzheimer's dementia. *Proc Natl Acad Sci USA*. 114:1690–1695.
- Power JD, Barnes KA, Snyder AZ, Schlaggar BL, Petersen SE. 2012. Spurious but systematic correlations in functional connectivity MRI networks arise from subject motion. *Neuroimage*. 59:2142–2154.
- Pozzi F, Di Matteo T, Aste T. 2012. Exponential smoothing weighted correlations. *Eur J Phys J B*. 85:175.
- Rousset OG, Ma Y, Evans AC. 1998. Correction for partial volume effects in PET: principle and validation. *J Nucl Med*. 39: 904–911.
- Schultz AP, Chhatwal JP, Hedden T, Mormino EC, Hanseeuw BJ, Sepulcre J, Huijbers W, LaPoint M, Buckley RF, Johnson KA, et al. 2017. Phases of hyperconnectivity and hypoconnectivity in the default mode and salience networks track with amyloid and Tau in clinically normal individuals. *J Neurosci*. 37:4323–4331.
- Serra L, Mancini M, Cercignani M, Di Domenico C, Spano B, Giulietti G, Koch G, Marra C, Bozzali M. 2017. Network-based

- substrate of cognitive reserve in Alzheimer's disease. *J Alzheimers Dis.* 55:421–430.
- Shirer WR, Ryali S, Rykhlevskaia E, Menon V, Greicius MD. 2012. Decoding subject-driven cognitive states with whole-brain connectivity patterns. *Cereb Cortex.* 22:158–165.
- Smith SM, Jenkinson M, Johansen-Berg H, Rueckert D, Nichols TE, Mackay CE, Watkins KE, Ciccarelli O, Cader MZ, Matthews PM, et al. 2006. Tract-based spatial statistics: voxelwise analysis of multi-subject diffusion data. *Neuroimage.* 31:1487–1505.
- Sole-Padullés C, Bartres-Faz D, Junque C, Vendrell P, Rami L, Clemente IC, Bosch B, Villar A, Bargallo N, Jurado MA, et al. 2009. Brain structure and function related to cognitive reserve variables in normal aging, mild cognitive impairment and Alzheimer's disease. *Neurobiol Aging.* 30:1114–1124.
- Sperling RA, Aisen PS, Beckett LA, Bennett DA, Craft S, Fagan AM, Iwatsubo T, Jack CR Jr., Kaye J, Montine TJ, et al. 2011. Toward defining the preclinical stages of Alzheimer's disease: recommendations from the National Institute on Aging-Alzheimer's Association workgroups on diagnostic guidelines for Alzheimer's disease. *Alzheimers Dement.* 7:280–292.
- Sperling RA, Bates JF, Chua EF, Cocchiarella AJ, Rentz DM, Rosen BR, Schacter DL, Albert MS. 2003. fMRI studies of associative encoding in young and elderly controls and mild Alzheimer's disease. *J Neurol Neurosurg Psychiatry.* 74:44–50.
- Sperling R, Mormino E, Johnson K. 2014. The evolution of preclinical Alzheimer's disease: implications for prevention trials. *Neuron.* 84:608–622.
- Stern Y. 2012. Cognitive reserve in ageing and Alzheimer's disease. *Lancet Neurol.* 11:1006–1012.
- Tang M, Ryman DC, McDade E, Jasielc MS, Buckles VD, Cairns NJ, Fagan AM, Goate A, Marcus DS, Xiong C, et al. 2016. Neurological manifestations of autosomal dominant familial Alzheimer's disease: a comparison of the published literature with the Dominantly Inherited Alzheimer Network observational study (DIAN-OBS). *Lancet Neurol.* 15:1317–1325.
- van Loenhoud AC, Wink AM, Groot C, Verfaillie SCJ, Twisk J, Barkhof F, van Berckel B, Scheltens P, van der Flier WM, Ossenkoppele R. 2017. A neuroimaging approach to capture cognitive reserve: application to Alzheimer's disease. *Hum Brain Mapp.* 38:4703–4715.
- Vandenberghe R, Van Laere K, Ivanoiu A, Salmon E, Bastin C, Triau E, Hasselbalch S, Law I, Andersen A, Korner A, et al. 2010. 18F-flutemetamol amyloid imaging in Alzheimer disease and mild cognitive impairment: a phase 2 trial. *Ann Neurol.* 68:319–329.
- Villemagne VL, Burnham S, Bourgeat P, Brown B, Ellis KA, Salvado O, Szoëke C, Macaulay SL, Martins R, Maruff P, et al. 2013. Amyloid beta deposition, neurodegeneration, and cognitive decline in sporadic Alzheimer's disease: a prospective cohort study. *Lancet Neurol.* 12:357–367.
- Villeneuve S, Rabinovici GD, Cohn-Sheehy BI, Madison C, Ayakta N, Ghosh PM, La Joie R, Arthur-Bentil SK, Vogel JW, Marks SM, et al. 2015. Existing Pittsburgh Compound-B positron emission tomography thresholds are too high: statistical and pathological evaluation. *Brain.* 138:2020–2033.
- Xia M, Wang J, He Y. 2013. BrainNet Viewer: a network visualization tool for human brain connectomics. *PLoS One.* 8:e68910.
- Yeo BT, Krienen FM, Sepulcre J, Sabuncu MR, Lashkari D, Hollinshead M, Roffman JL, Smoller JW, Zollei L, Polimeni JR, et al. 2011. The organization of the human cerebral cortex estimated by intrinsic functional connectivity. *J Neurophysiol.* 106:1125–1165.
- Yu Q, Erhardt EB, Sui J, Du Y, He H, Hjelm D, Cetin MS, Rachakonda S, Miller RL, Pearlson G, et al. 2015. Assessing dynamic brain graphs of time-varying connectivity in fMRI data: application to healthy controls and patients with schizophrenia. *Neuroimage.* 107:345–355.
- Zalesky A, Fornito A, Bullmore ET. 2010. Network-based statistic: identifying differences in brain networks. *Neuroimage.* 53:1197–1207.
- Zalesky A, Fornito A, Cocchi L, Gollo LL, Breakspear M. 2014. Time-resolved resting-state brain networks. *Proc Natl Acad Sci USA.* 111:10341–10346.
- Zhang M, Li J, Chen C, Xue G, Lu Z, Mei L, Xue H, Xue F, He Q, Wei M, et al. 2014. Resting-state functional connectivity and reading abilities in first and second languages. *Neuroimage.* 84:546–553.